RSC Applied Polymers

Accepted Manuscript

This article can be cited before page numbers have been issued, to do this please use: A. Tripathy, J. P. Das, S. Balasubramaniam, S. Kim and A. Ramadoss, *RSC Appl. Polym.*, 2026, DOI: 10.1039/D6LP00034G.

ROYAL SOCIETY OF CHEMISTRY

rsc.li/RSCApplPolym

View Article Online
DOI: 10.1039/D6LP00034G

Standalone 3-D Piezoelectric Polymer-Ceramic Foam for Efficient Energy Harvesting

Alekhika Tripathy[1$], Jyoti Prakash Das[2$], Balasubramaniam Saravanakumar[1], Sang Jae Kim[2], Ananthakumar Ramadoss[3$*]

[1]School for Advanced Research in Polymers: Laboratory for Advanced Research in Polymeric Materials (LARPM), Central Institute of Petrochemicals Engineering and Technology (CIPET), Bhubaneswar-751024, India.
[2]Nanomaterials and Systems Lab, Major in Mechatronics Engineering, Faculty of Applied Energy System, Jeju National University, Jeju, 63243, South Korea.
[3]School for Advanced Research in Polymers: Advanced Research School for Technology & Product Simulation, Central Institute of Petrochemicals Engineering & Technology, Guindy, Chennai - 600032, India.

……

*Corresponding Author

Email: ananth.cipet@gmail.com / ananth@cipet.gov.in (A. Ramadoss)

ORCID Ananthakumar Ramadoss: 0000-0002-6616-7693

$ These authors contributed equally

Abstract

The rising demand for wearable electronics has drawn widespread attention to piezoelectric materials due to their potential applications in low-power devices. Herein, we present a unique method for fabricating free-standing foam-structured piezoelectric nanogenerators (PENGs) with excellent piezoelectric response using polyvinylidene fluoride (PVDF) embedded with piezoceramics. The as-fabricated foam with porous structure and good flexibility delivered a maximum piezoelectric peak-to-peak output voltage and current of 11.61 V and 70 nA. Both PVDF and the integrated ceramic nanoparticles in the composite foams contribute to the piezoelectric performance, thus giving better output as compared to the pristine PVDF foam. Moreover, the interconnected pores within the foam structure provide a high surface area engendering the material with good amount of stress concentration sites that help in improving the piezoelectric voltage, respectively. This work presents a convenient

View Article Online
DOI: 10.1039/D6LP00034G

method for designing mechanical energy harvesters that has great potential in self-powered wearable electronic devices.

Keywords: Piezoelectric Foam, 3D-Structure, Wearable Energy Harvester, Lead-Free, Sacrificial Template

1. Introduction

Mechanically flexible piezoelectric materials are in considerable demand for use in energy-scavenging devices [1-8]. However, these two characteristics, piezoelectricity and mechanical flexibility, are incompatible since they cannot be enhanced simultaneously. Although polymers like PVDF possess mechanical flexibility and ease of processing, their piezoelectric coefficients are substantially lower than those of piezoelectric ceramics [9-14]. The latter, with high piezoelectric coefficients, cannot be fabricated in mechanically compliant structures because mechanical strain rapidly fractures them. So, in order to produce mechanically flexible structures, several topologies such as thin films and nanowire arrays using piezoelectric ceramics and semiconductor oxides have been investigated recently. The processing techniques of these one-dimensional (1D) and two-dimensional (2D) nanostructures not only pose constraints for large-scale production but are also cost-intensive. Another demerit of these lower dimensional structures is that they have limited loading directions that are responsible for the piezoelectric effect. Henceforth, constructing higher-order structures with substantial mechanical flexibility is critical for applications such as acoustic transducers, wearable electronic devices, compact energy harvesters, and so on.

Most of the traditional piezoelectric nanogenerators (PENGs) are 2D structures which fail to amplify the piezoelectric output. The primary reason behind this is that the 2D structures do not consider normal strains but only the transverse and longitudinal strains [15, 16], whereas

View Article Online
DOI: 10.1039/D6LP00034G

in a 3D structure, the total space contributes towards generating the larger piezoelectric strain [17]. Therefore, many research works have been carried out on 3D energy harvesters as listed in the comparison table in a later section. These works clearly show that as compared to planar structures, the piezoelectric output voltage of 3D structures are many times higher. In particular, unlike bulk materials, materials with porous structure results in lesser volume and lower modulus, and hence acquires larger compression strain thereby generating higher piezoelectric output [18-20]. Generally, porous structures are more flexible as compared to bulk materials. Due to this, applying a similar force can generate larger strain and voltage output in a porous material than in a bulk one [21]. Beyond offering flexibility, the enhanced piezoelectric performance of these foamed porous structures arises from a synergistic interaction between the material's components and its architecture. In particular, the large surface area of interconnected pores serves as stress concentration sites, intensifying localized deformation and thereby maximizing the piezoelectric energy output [22].

In the case of piezoelectric ceramics, the relative permittivity decreases with increasing porosity. This can be attributed to the simultaneous increase in surface area and space-charge fields based on the space-charge theory [23]. Till date, many research works have been conducted to introduce porosity into the dense material in order to reduce the permittivity of the sensor material [24-27]. Piezoelectric sensitivity might increase in devices with better piezoelectric symmetry, which could lead to a variety of fascinating applications. Foams are such structures, which are made up of materials packed in a random network with a high void proportion. Conventionally, piezoceramics are used in developing such piezoelectric materials via robocasting [28] or fused-deposition [29] techniques that can prepare porous structures layer-by-layer or by polymer templating. Lead zirconate titanate (PZT)-based foams have been discovered to have lower acoustic impedance, greater mechanical flexibility, and higher piezo-sensitivity than other thin films, and have thus been employed in a variety of applications such

View Article Online
DOI: 10.1039/D6LP00034G

as actuators, wide-band hydrophones, and so on [30, 31]. Even though the porous structure improves the mechanical and electrical capabilities of the piezoceramics, they remain fragile.

For this purpose, piezoelectric polymers are widely being integrated so that they can maintain an isotropic mechanical integrity along with merits like higher elasticity, biocompatibility, easy processability, etc. In addition to its cost-effective synthesis methods they also offer good piezoelectric output. PVDF is a well-known piezoelectric material with a piezoelectric coefficient of d_{33} ranging from 20 to 34 pC/N. Although its coefficient is considerably lower than that of piezoceramics, PVDF is commonly used in a wide range of applications because of its favorable mechanical and electrical properties. PVDF has been electrospun into fibres to improve its integration capability and flexibility, allowing it to be employed in applications such as hydrophones [32], acoustic transmitters [33], nonvolatile low-voltage memory [34], implantable medical devices [35], and so on. There are numerous reported works involving the production of PVDF foams for efficient energy harvesters [27, 36]. In this study, PVDF polymer was utilized to develop the foam structure. As a result, numerous piezoelectric composite foams exhibiting excellent flexibility and strong piezoelectric performance have been produced. These foam structures are obtained via different methods, such as sol-gel [37] by the addition of foaming additives [38], or by the use of supercritical carbon dioxide [39], etc.

This work reports achieving a highly porous foam structure that is exceedingly soft and flexible through a simple and scalable process. In order to simultaneously obtain a significant piezoelectric output and retain structural isotropy, this work presents the development of a highly elastic piezoelectric composite-based foam structure using PVDF and ceramics like $BiFeO_3$ (BFO) and $K(Na, Nb)O_3$ (KNN), providing a comprehensive evaluation of their piezoelectric performance. The composite foam was fabricated by molding a PVDF–piezoelectric nanoparticle (NP) dispersion within a sacrificial nickel (Ni) framework.

View Article Online
DOI: 10.1039/D6LP00034G

Subsequent removal of the Ni template resulted in a well-interconnected foam structure with well-dispersed constituents.

2. Experimental Section

2.1 Materials

The starting materials used in the synthesis of BFO and KNN include Bi $(NO_3)_2.6H_2O$ (Sigma Aldrich Pvt. Ltd.), Fe $(NO_3)_3.9H_2O$ (Himedia Pvt. Ltd.), Nitric acid (Himedia Pvt. Ltd.), Nb_2O_5 (Himedia Pvt. Ltd.), KOH (Himedia Pvt. Ltd.) and NaOH (Himedia Pvt. Ltd.). For foam fabrication, the materials used were PVDF powder (Sigma Aldrich, India), N, N-dimethyl formamide (DMF) procured from SRL Chem, India, and Nickel foam (Taiwan, 2 mm thickness, 95% porosity).

2.2 Preparation of PVDF-based Piezoceramics Composite Foams via Template-Assisted Process

The PVDF-based composite foams were prepared as per the following procedure. The piezoceramics, such as BFO and KNN NPs, were synthesized by hydrothermal process. The detailed procedure for the syntheses of piezoceramic NPs are given in the supporting information (SI). The optimized weight percentage (6 wt%) of PVDF was added to the DMF solvent in a beaker and then stirred at 60°C at 400 rpm for 3 hrs to ensure complete dispersion of the particle within the solution. After its complete dissolution in the solvent, piezoceramic NPs in the compositions 2 and 4 wt % were added to the solution accordingly and stirring was continued for two hours. The composite foams were named as PVDF-BFO-2wt%, PVDF-BFO-4wt%, PVDF-KNN-2wt% and PVDF-KNN-4wt%, respectively. A Ni foam (5 cm × 3 cm) was taken and dipped in the prepared solution. It was then dried at 60°C in the oven. After the foam was completely dried, it was again properly dipped into the solution and then dried under the same conditions. This dipping and drying process was repeated multiple times to achieve the compactness of the composite foam. The weight of the foam before and after the

View Article Online
DOI: 10.1039/D6LP00034G

dipcoating was measured. Further, to obtain a porous structured PVDF nanocomposite framework, Ni was etched out by immersing that foam in a concentrated HNO_3 solution (pH ~ 4), followed by rinsing the foam in DI water and drying at 60 ℃. Then the weight of the foam was measured and it was found that > 95% of Ni was removed. The average thickness of the foam samples was 1.8 mm. The pristine PVDF foam was also fabricated by dipping the Ni foam in the first solution without the addition of ceramics, and then the same procedure was followed to obtain the pure PVDF foam. Finally, different types of 3D foam structures were obtained (PVDF and Composite foam). The schematic of the preparation technique of the foam and its electrical measurement set-up is shown in **Figure 1a-b**.

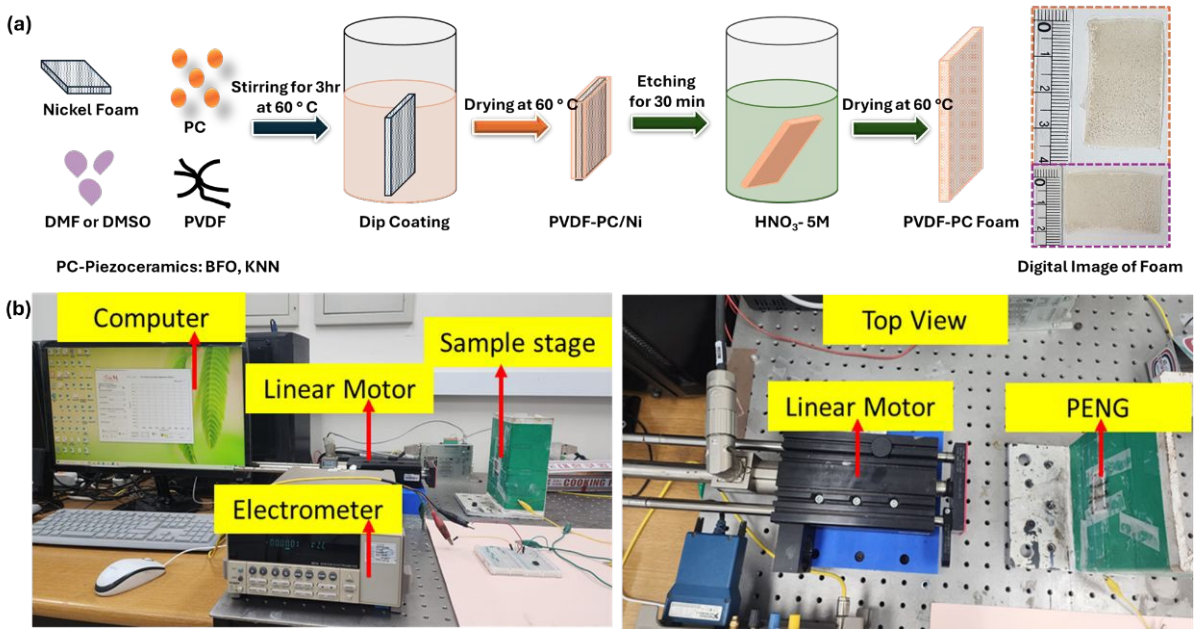

Figure 1. (a) Schematic illustration of the fabrication process of PVDF-piezoceramic composite foam and (b) Digital images of the energy harvesting set-up, including linear motor, electrometer and the software interface of the control system.

2.3 Fabrication and Testing of PENG device based on PVDF-based Piezoceramic Composites foam

The piezoelectric nanogenerator (PENG) was fabricated using the as-prepared piezoelectric foams (PVDF, PVDF-KNN, and PVDF-BFO) with chromium and gold as top

View Article Online
DOI: 10.1039/D6LP00034G

and bottom electrodes deposited via magnetron sputtering (Current: 20 mA; Time: 120s; Temperature: RT; Gas: Argon) followed by encapsulating with antistatic tape (to avoid any contact resistance or external disturbance). The copper wires were connected to both sides of the electrodes for measurements. Before electrical measurements, the devices were poled at 5kV for 30 min via electrode poling set-up. The open-circuit voltage and short-circuit current were measured at various load resistances (1MΩ to 1.1 GΩ) using Electrometer 6514 with force applied via a linear motor. The applied compressive force is roughly 2 N, given a moving mass of about 2 kg and an operating acceleration of 1 m/s².

3. Results & Discussion

3.1 Physicochemical Characterization

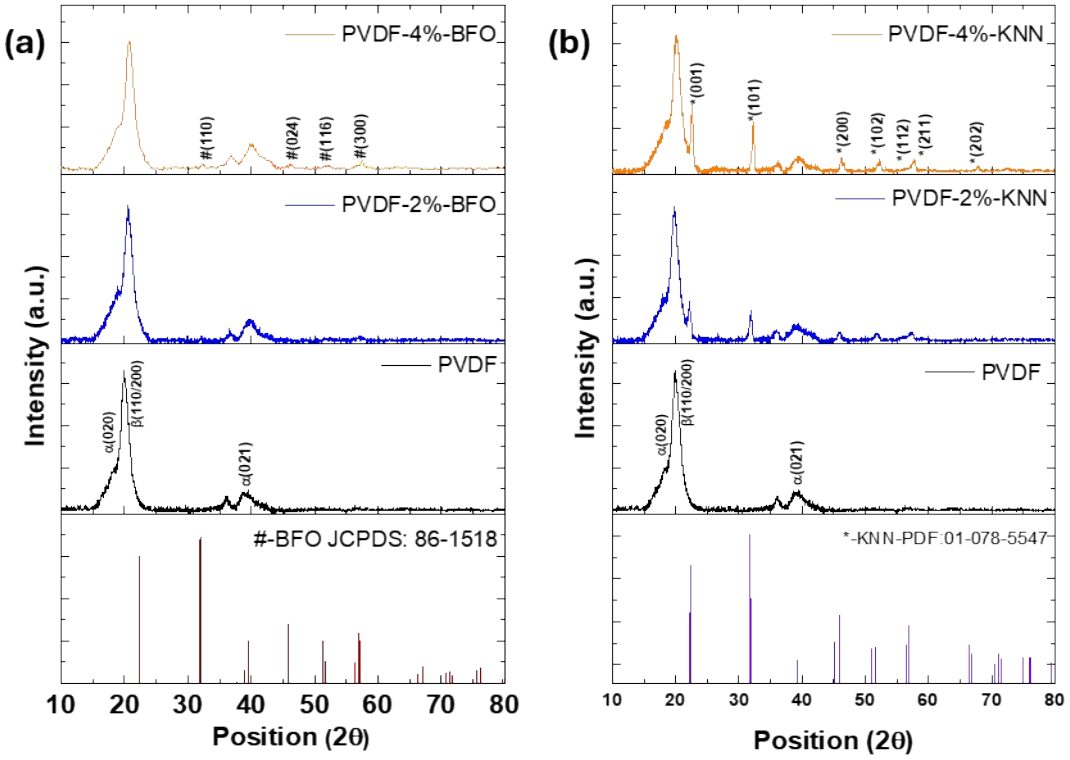

Figure 2. XRD spectra of the (a) PVDF-BFO and (b) PVDF-KNN foams with pristine PVDF

The XRD pattern of the fabricated foams is shown in **Figure 2a-b.** The major peak at ~20° corresponds to the (110) and (200) diffraction planes of the β phase. The peaks

corresponding to BFO (**Figure 2a**), and KNN (**Figure 2b**) are represented as '#'. The characteristic diffraction planes corresponding to the synthesized BFO and KNN are clearly indexed in the figure confirming that they exhibit a rhombohedral distorted perovskite structure, and a tetragonal perovskite structure, respectively. The observed diffraction peaks of the ceramic fillers were exactly matched with the JCPDS card no. 86-1518, and PDF no. 00-065-0276 for BFO and KNN, respectively. Further, the calculated degree of crystallinity values for PVDF, PVDF–2%BFO, PVDF–4%BFO, PVDF–2%KNN, and PVDF–4%KNN electrodes were found to be approximately 79%, 81%, 83%, 82%, and 85%, respectively. The results indicate a gradual increase in crystallinity with increasing filler content, confirming the role of ceramic fillers as effective heterogeneous nucleating agents.

Figure 3a-b depicts the FTIR spectra of the various fabricated foams. It shows that the composite foams consist of α and β-phases. The absorption peaks at 873 and 1166 cm^{-1} occur due to the presence of β-phase. The peak at 871 cm^{-1} corresponds to the CF_2 stretching and CH_2 rocking vibrations whereas the peaks at 1070, 1165, and 1400 cm^{-1} are due to the CF_2 stretching, C-C skeleton, and CH_2 deformation generated by the rocking vibrations. The absorption bands at 840 cm^{-1} (CF_2 rocking) and 1400 cm^{-1} (CH_2 bending) are a characteristic of the β-phase whereas the band at 762 cm^{-1} (skeletal bending and CF_2 bending) correspond to α-phase, respectively. Further, using the Beer-Lamberts law, β-phase fraction percentage (F(β)) was estimated. It was observed that the F(β) value increased from 75.2% to 76.3% for PVDF-2%-BFO and PVDF-4%-BFO. Similarly, the value increased from 70.8% for PVDF-2%-KNN to 71.3% for PVDF-4%-KNN. Thus, an enhancement in β-phase value with an increase in filler content confirms that the β-phase value improved after the addition of ceramic fillers in the foam. Although only a slight increase in β-phase content is observed, the incorporation of high piezoelectric ceramic fillers significantly enhances the overall

View Article Online
DOI: 10.1039/D6LP00034G

performance due to synergistic effects arising from improved crystallinity, efficient stress transfer, and strong interfacial interactions, rather than β-phase content alone.

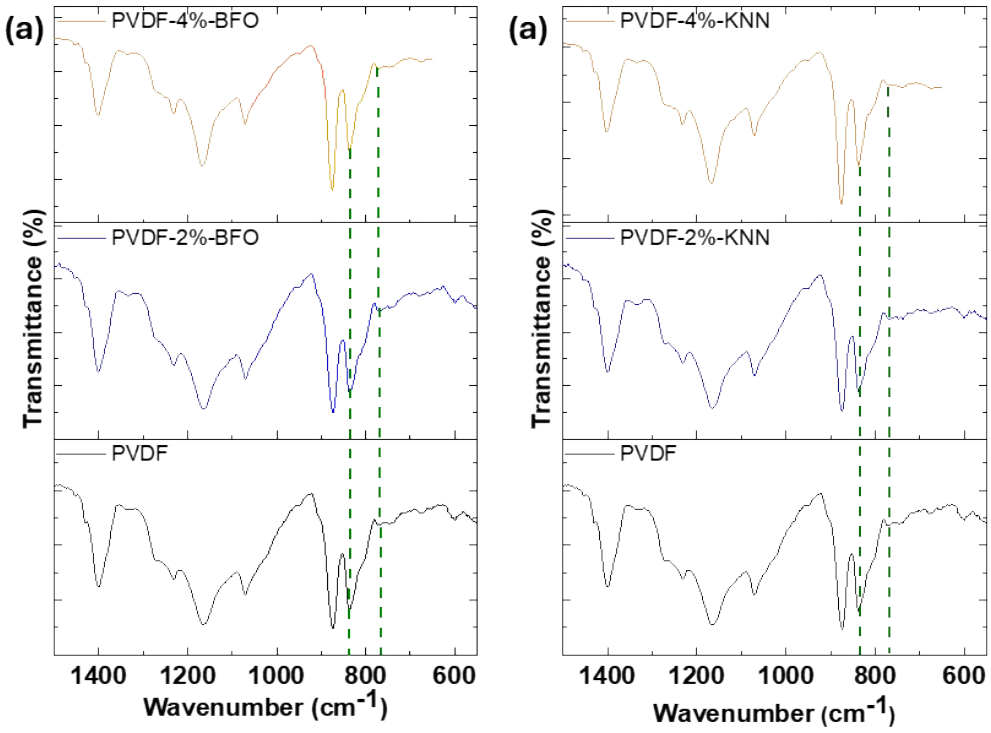

Figure 3. FTIR spectra of the (a) PVDF-BFO and (b) PVDF-KNN foams with pristine PVDF

FE-SEM analysis was used to observe the morphology of the developed foams. In **Figure S1a-b** the FE-SEM images of the synthesized BFO and KNN nanoparticles reveal an agglomerated structure. The average particle size of BFO and KNN nanoparticles was approximately 300 nm and 500 nm, respectively. As inferred from the FE-SEM micrographs (**Figure 4**), the fabricated polymer composite foams exhibit an honeycomb-like structure with many open gaps on the surface, with the NPs clearly embedded in the PVDF matrix (**Figure.4a-d**), resulting in a well-integrated structure with an interconnected foam architecture and uniformly dispersed constituents. The illustrated FE-SEM micrographs confirms existance of an open-cell, interconnected porous structure with continuous pore channels and no isolated

View Article Online
DOI: 10.1039/D6LP00034G

void. In line with the improved electromechanical response mentioned, this demonstrates the existence of a flexible and compressible network that promotes effective stress transfer. Crucially, all samples exhibit comparable microstructural characteristics within each composition, suggesting minimal batch-to-batch variance and adequate control over synthesis conditions. Therefore, the findings of the FE-SEM micrographs verify the development of a porous structure in the foam samples and the even dispersion of the NPs throughout the PVDF matrix.

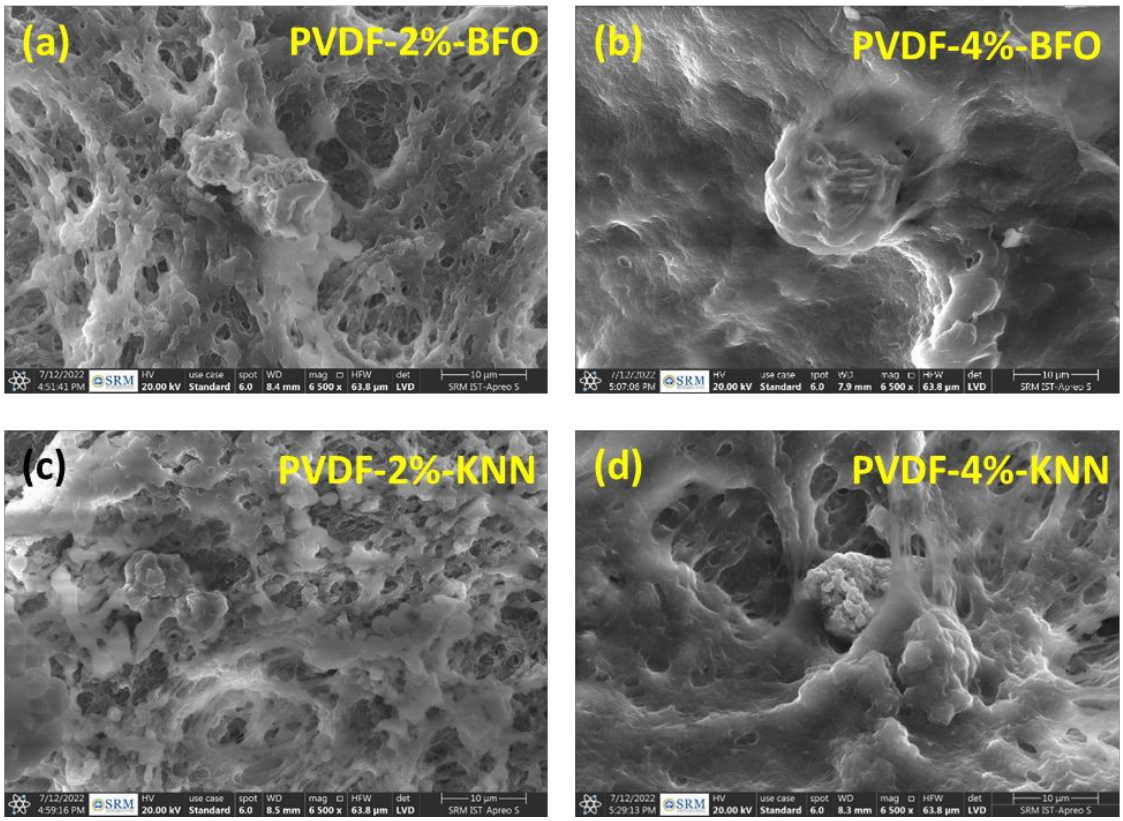

Figure 4. FESEM micrographs of the composite foams (a) PVDF-2%-BFO, (b) PVDF-4%-BFO, (c) PVDF-2%-KNN, and (d) PVDF-4%-KNN.

Figure 5a-d displays the EDS spectrum of the PVDF-2%-BFO, PVDF-4%-BFO, PVDF-2%-KNN, and PVDF-4%-KNN foams. The atomic percentages of the C, O, F, Bi, and Fe elements in the PVDF-2%-BFO foam (**Figure 5a**) were 22.11, 18.71, 50.94, 4.88, and 3.36%, respectively. The C, O, F, Na, K, and Nb elements were detected in the PVDF-2%-KNN foam (**Figure 5c**) with atomic percentages of 26.78, 18.23, 40.82, 7.51, and 6.46%, respectively. The

View Article Online
DOI: 10.1039/D6LP00034G

elemental composition of the PVDF-4%-BFO (**Figure 5b**) and PVDF-4%-KNN foams (**Figure 5d**) was confirmed by EDS analysis as well. Further, **Figure S2-S5** shows the EDS mapping of PVDF-2%-BFO, PVDF-4%-BFO, PVDF-2%-KNN and PVDF-4%-KNN foams, where the elements such as F, C, Bi, Fe and O for PVDF-BFO and F, C, K, Na, N, and O for PVDF-KNN confirm the uniform distribution of the piezoceramics (BFO and KNN) in the polymeric (PVDF) matrix. The limited distribution is attributed to the low filler content (2% and 4%) compared to the polymer matrix (98% and 96%). Further, no traceable amount of Ni was observed from the EDS analysis, which confirms the complete etching of Ni. Thus, the EDS results confirmed the presence of the fillers in the fabricated composite foams.

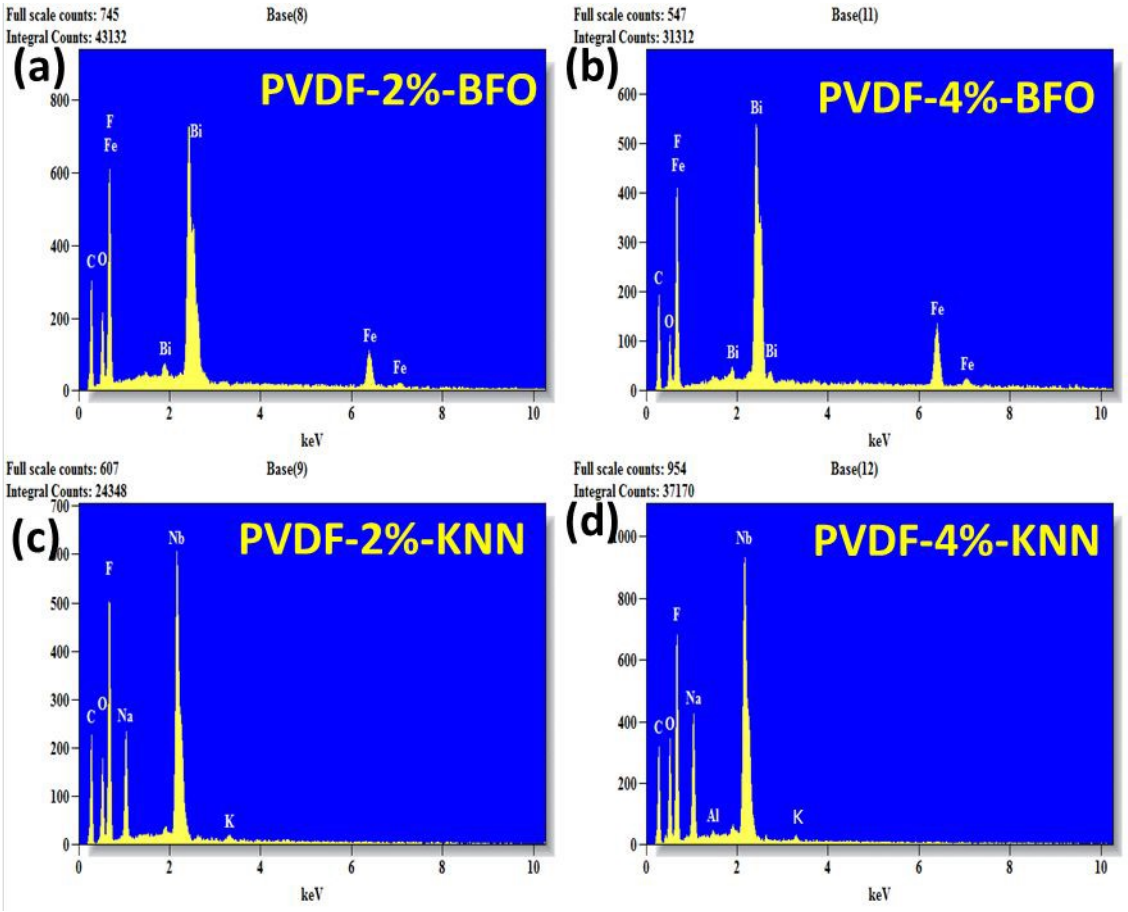

Figure 5. EDS spectra of (a) PVDF-2%-BFO, (b) PVDF-4%-BFO, (c) PVDF-2%-KNN and (d) PVDF-4%-KNN foams

View Article Online
DOI: 10.1039/D6LP00034G

The DSC analysis was performed to investigate the melting behaviour of the fabricated pristine and composite foam structures. **Figure S6** shows the DSC heating curves for the pristine PVDF and the composite foams with varying weight fractions of fillers. **Figure S6a** indicates that the pure PVDF foam exhibits a melting temperature at about 161.5 °C with a small endothermic peak at a lower temperature (106 °C). The melting temperature of the α-phase PVDF is lower than that of the β-phase. This type of melting behavior arises due to double melting transitions very often observed in PVDF owing to its polymorphic structure. The first peak represents the melting of the α-phase, while the second peak at 161.5 °C is assigned to the β-phase of PVDF crystals. In case of the composite foams, there is only one peak for each of the PVDF-BFO (**Figure S6a**) and PVDF-KNN (**Figure S6b**) foams. In case of PVDF-BFO foams, the melting temperature is located at 164.5, and 160.9 °C for composites containing 2 and 4 wt% of BFO, respectively. Similarly, for PVDF-2%-KNN and PVDF-4%-KNN, the melting peaks are at 164.5 and 162.7 °C. It was observed that the melting point increased with the addition of 2wt% filler in the PVDF composite foam. This feature can be attributed to the better dispersion of the NPs in the polymer matrix at a low filler loading, which promotes heterogeneous nucleation and facilitates the formation of more ordered crystalline domains. However, further increasing the filler loading to 4% leads to the a decrease in the melting temperature, which may be due to the formation of imperfect crystalline domains and possess reduced lamellar thickness. The high filler concentration induces interfacial constraints and limits polymer chain mobility, resulting in the formation of smaller and thermally less stable crystals. The TGA curves of the various foams are depicted in **Figure S6c-d.** TGA analysis was performed to determine the thermal stability of the foams. It shows that the amount ultimately left over after foam degradation is higher for composite foams than for virgin PVDF foam. Furthermore, it is evident that as the filler content increased, the weight percentage after

View Article Online
DOI: 10.1039/D6LP00034G

degradation rises, supporting the proper growth of composite foams matching to filler weight percentage.

The practical load-bearing and flexibility of the PVDF composite foam was assessed by calibrated load cell, as shown in **Figure 6**. The composite foam exhibited better structural integrity and elastic recovery, with no discernible deformation or fracture when loaded incrementally from 50 g to 250 g. This experiment confirms the material's suitability for wearable applications, where routine handling and moderate mechanical stresses are expected.

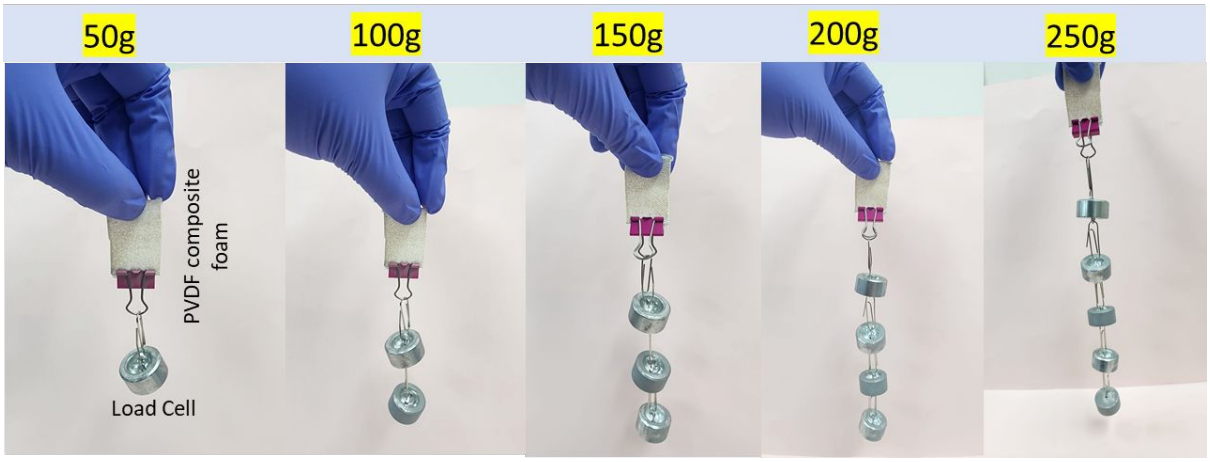

Figure 6. Digital images of load-bearing test for the PVDF composite foam

3.2 Piezoelectric Property Analysis

The previous section illustrated the device fabrication process. **Figure 7a** depicts the digital image of the fabricated device. The poled composite foams were used to fabricate a PENG. The as-fabricated device was tested under the impact of a force generated by a linear motor. Mechanical energy that was applied to the nanogenerator was transformed into useable electrical energy that could be stored and used to power low-power devices later. The open-circuit voltage and short-circuit current, measured under the impact of a 1 m s^{-2} acceleration at various load resistances from 1MΩ to 1.1 GΩ, are shown in **Figures S7a-d and S8a-d,** respectively.

View Article Online
DOI: 10.1039/D6LP00034G

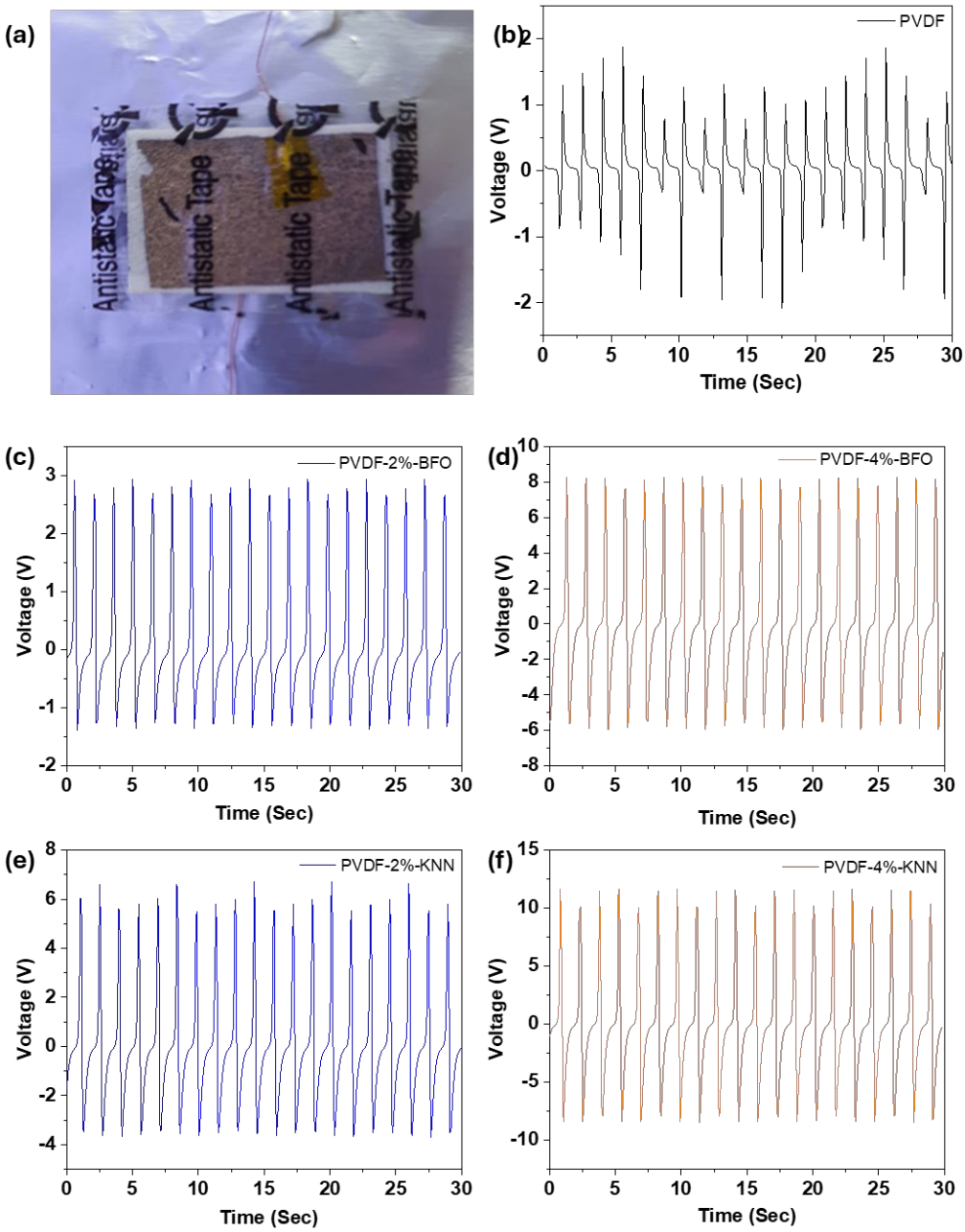

Figure 7. (a) Digital image of the fabricated foam-based PENG device. Open circuit voltage of (b) PVDF, (c) PVDF-2%-BFO, (b) PVDF-4%-BFO, (c) PVDF-2%-KNN and (d) PVDF-4%-KNN foam-based PENG devices at 1 GΩ.

View Article Online
DOI: 10.1039/D6LP00034G

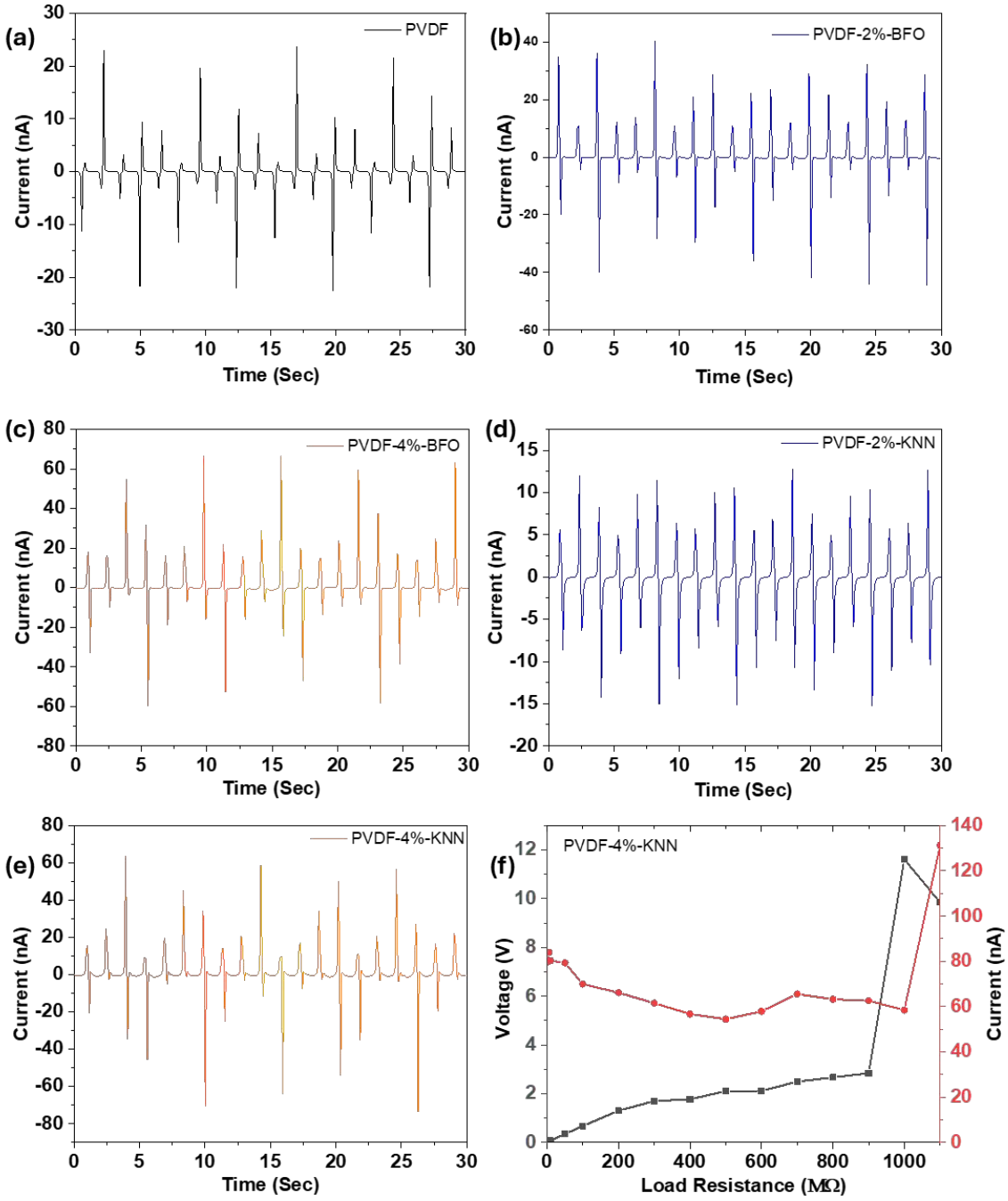

Figure 8. Output current generated by the (a) PVDF, (b) PVDF-2%-BFO, (c) PVDF-4%-BFO, (d) PVDF-2%-KNN and (e) PVDF-4%-KNN foam-based PENG devices at 1GΩ. (f) Open circuit voltage and short-circuit current of PVDF-4%-KNN foam-based PENG devices at various load resistances

View Article Online
DOI: 10.1039/D6LP00034G

The output voltage and current (**Figures 7b and 8a**) of the pristine PVDF foam is 3.78 V and 45 nA, respectively. As can be seen in **Figure 7c-d,** PVDF-2%-BFO foam gives an output voltage of about 2.95 V whereas PVDF-4%-BFO generates a higher voltage of ~ 8.35 V. Similarly, in the case of PVDF-2%-KNN and PVDF-4%-KNN based PENG, the output voltage increases with increased loading of KNN NPs in PVDF-2%-KNN and PVDF-4%-KNN delivering ~ 6.73 V and 19.5 V, respectively (**Figure 7e-f)**. Thus, for both types of foams, it is observed that the output voltage increases with increasing filler content. Also, the PVDF-4%-KNN foam-based PENG device produced the maximum output voltage of ~11.61 V at 1 GΩ load resistance, indicating that 1 GΩ is the matching load resistance for the device. Further, **Figure 8** shows the current generated by the composite foams. PVDF-2%-BFO and PVDF-4%-BFO foam-based PENGs (**Figure 8b-c)** deliver an output current of ~35 nA and 66 nA, respectively, whereas for the foams PVDF-2%-KNN and PVDF-4%-KNN (**Figure 8d-e)** the values are ~13 nA and 70 nA, respectively. It is observed that the output voltage of the composite foam is higher (Difference ~7.83 V and 25 nA) than that of the pristine foam, and also, the performance increases with increasing filler content. Moreover, it is observed that the PVDF-KNN foam-based PENGs deliver better output voltage than the PVDF-BFO-based PENGs, and the forward and reverse bias characteristics of the PVDF-4%-KNN device are shown in the **Figure S9a-b**. The output performance of the fabricated foam-based PENG devices was compared to that of the recently reported PVDF and its copolymer-based composite nanogenerators (**Table 1**). It can be clearly observed that the filler content in the reported works is higher than that used in the current work. Thus, the 3D porous foam structure offers a continuous pathway for easy transfer of load and hence results in better performance.

View Article Online
DOI: 10.1039/D6LP00034G

Table 1 Comparison of the current work with similar recent works

PENG Material	Output Voltage (V)	Output Current (nA)	References
PVDF-MWCNT Foam	12 V	30	[40]
PDMS-BTO-MWCNT Foam	1.5 V	-	[27]
PVDF Foam	7 V	75	[41]
PVDF/ZIF-8 Foam	10 V	90	[42]
PVDF Foam	4.1	70	[43]
Polypropylene Foam	5.7	-	[44]
PVDF Foam	4.7	43.6	[45]
PVDF Foam	11.84	217.78	[36]
PVDF Foam	19.1	580	[46]
PVDF-BT Foam	12.5	150	[39]
PVDF Foam	3.78	45	Present work
PVDF-BFO Foam	~ 8.35	~ 66	Present work
PVDF-KNN Foam	~ 11.61	~ 70	Present work

View Article Online
DOI: 10.1039/D6LP00034G

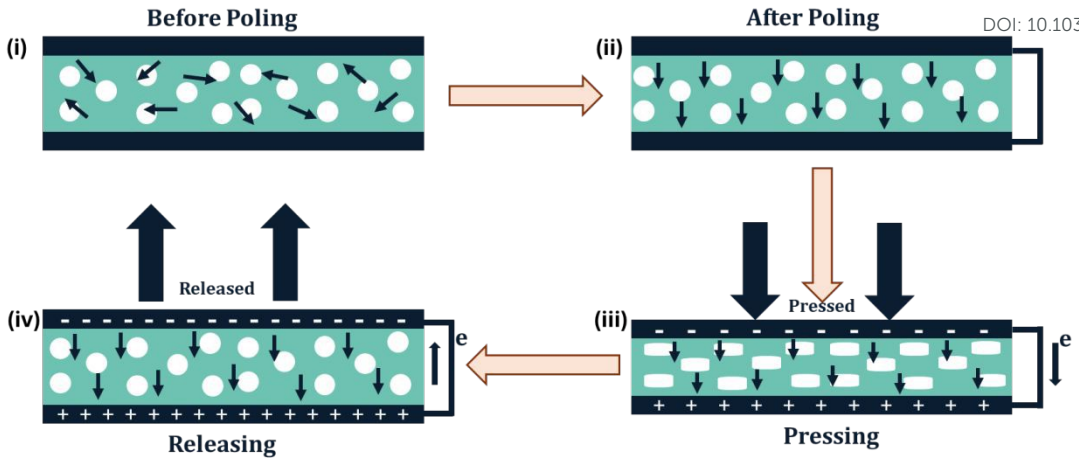

Figure 9. Schematic diagram of the operating mechanism of PENG

Figure. 9 depicts a schematic representation of the PENG's internal functioning mechanism. (i) The dipoles in the piezoceramic materials are initially arranged arbitrarily when no poling is present, (ii) When an electric field is applied to the device, the dipoles will align themselves in the direction of the field. When there is no impact from a human palm, there is no development of an electric signal, and it remains in a state of balance, (iii) The piezoelectric potential is created between the electrodes of the device as a result of the compressive strain that is caused by the application of a human palm impact to the device. An AC output signal is produced while this operation is being carried out. (iv) Finally, a tiny flexible force that emerges after releasing a palm hit produces a reverse piezoelectric potential.

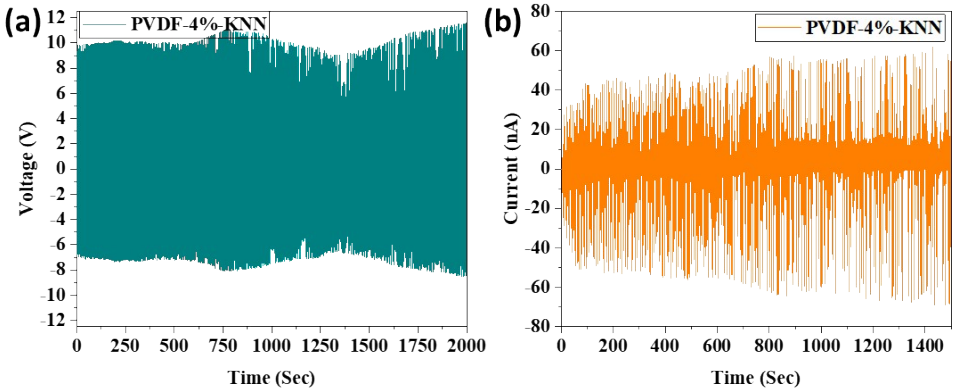

Figure 10. Stability tests of PVDF-KNN devices: (a) output voltage and (b) current

View Article Online
DOI: 10.1039/D6LP00034G

Further, the long-term stability of the PVDF-2%-BFO, PVDF-4%-BFO, PVDF-2%-KNN (**Figure S10a-c**) and PVDF-4%-KNN (**Figure 10a-b)** foam-based PENG devices for 600 seconds at an impact of an acceleration of 1 m s^{-2} was tested. It showed almost constant peak-to-peak voltage throughout the 400 consecutive cycles, which indicates the better performance of the fabricated composite devices. In addition, a commercial capacitor with a capacity of 0.22 μF was used to test the PENG's ability to charge capacitors. It is observed that the charging voltage increased at an exponential rate, reaching its maximum value of 2.0 V in approximately 165 seconds. This was done by charging the capacitor with the rectified output that was acquired from a bridge rectifier (**Figure 11a**). The PENG was connected with green LEDs in the absence of any energy storage device in order to determine whether or not it would be useful for real-world applications. The PENG was able to instantaneously light up the green LEDs (**Figure 11b**) whenever they were subjected to the impact of finger tapping. In addition, the charging pattern of the capacitor using the PENG is displayed in **Figure 11c**, which depicts the pressing and releasing modes of operation. Further, the feasibility of the as-fabricated PENG device as a biomechanical energy harvester was tested under different conditions (Finger, foot, palm tapping, and elbow bending), by placing a device in the body (**Figure 11d**). The foot tapping-based biomechanical energy exhibited higher output compared to other body motions. The applied force during various actuation modes was quantitatively measured using a pressure sensor, as shown in **Figure S11.** The average forces recorded during finger, palm, and foot tapping were approximately 10 N, 20 N, and 35 N, respectively. The acquired results confirmed that the composite devices outperformed the pristine devices in terms of output. The results show that the output voltage increases as piezoceramic KNN content in the foam rises from 2wt% to 4wt%. These findings support the possible use of foam-based PENG as a biomechanical energy harvester in a variety of settings, including toll booths, as well as for

View Article Online
DOI: 10.1039/D6LP00034G

various motion sensors used in biomedical devices, traffic monitoring systems, tactile sensors, wireless sensors, etc.

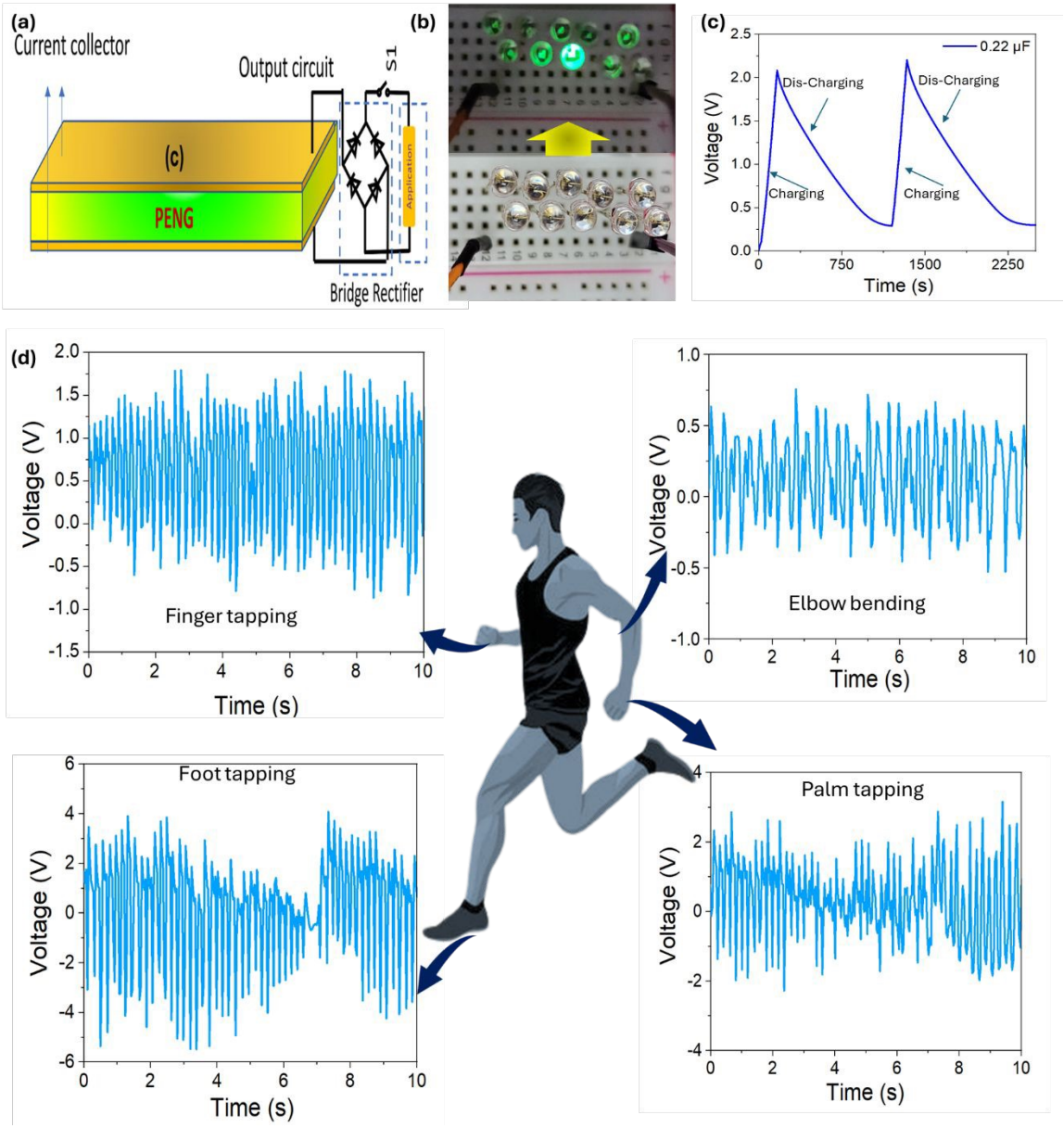

Figure 11. (a) Rectifier circuit, (b) light up the green LEDs, and (c) charging pattern of the capacitor via a foam-based PENG device. (d) Generating voltage under various biomechanical movements: Finger tapping, Elbow bending, Foot tapping, and Palm tapping.

View Article Online
DOI: 10.1039/D6LP00034G

4. Conclusion

In summary, a simple and scalable approach was used to create a flexible, lightweight, lead-free ceramic polymer composite foam. The ultimate aim was to develop a structure with low weight and high compliance. In this context, the piezoelectric foam was fabricated via casting a sacrificial nickel framework with PVDF-ceramic NPs (BFO and KNN) dispersed, followed by an etching of the Ni template. Furthermore, the porous nature of the fabricated foams can directly impact their piezoelectric activity. The composite-based PVDF-KNN device exhibited greater piezoelectric output voltage and current of 11.61 V and 70 nA when compared to pristine PVDF foam. The foam devices also demonstrated good stability, which helps their practical application in a variety of applications. Despite the low filler weight fraction, the PENG demonstrates better performance compared to conventional composite films, owing to its 3D interconnected architecture, which facilitates continuous load transfer, which is difficult to achieve in low-filler conventional composites. Thus this work presents a scalable ceramic–polymer composite based on an interconnected 3D piezoelectric foam structure, and the results highlight a novel material platform for self-powered micromechanical devices and efficient energy harvesting applications.

Supporting Information

Synthesis of BFO and KNN nanoparticles, characterization methods, FESEM of BFO and KNN nanoparticles, EDS mapping, PENG evaluation of the prepared PVDF and PVDF composite foam devices.

Acknowledgments

The authors acknowledge the funding by the Department of Science and Technology (Ref. SP/YO/2019/1432), Government of India for the research work.

Declaration of competing interest

View Article Online
DOI: 10.1039/D6LP00034G

The authors declare having no known competing financial interest or personal relationship that could influence the work reported in this paper.

Data availability

The data supporting this article have been included as part of the Supplementary Information.

References

[1] S. Park, H. Kim, M. Vosgueritchian, S. Cheon, H. Kim, J.H. Koo, T.R. Kim, S. Lee, G. Schwartz, H. Chang, Z. Bao, Stretchable Energy-Harvesting Tactile Electronic Skin Capable of Differentiating Multiple Mechanical Stimuli Modes, Advanced Materials, 26 (2014) 7324-7332.

[2] F.R. Fan, W. Tang, Z.L. Wang, Flexible Nanogenerators for Energy Harvesting and Self-Powered Electronics, Advanced Materials, 28 (2016) 4283-4305.

[3] H. Wu, Y. Huang, F. Xu, Y. Duan, Z. Yin, Energy Harvesters for Wearable and Stretchable Electronics: From Flexibility to Stretchability, Advanced Materials, 28 (2016) 9881-9919.

[4] Z. Chen, H. Yang, H. Yu, T. Yu, L. Liu, Y. Lu, W. Gao, PVDF/PANi@HNT Nanocomposite Membranes: Pioneering Solutions for Piezoelectric Sensing and Energy Harvesting Efficiency, ACS Applied Materials & Interfaces, 17 (2025) 28668-28681.

[5] D.K. Bharti, S. Kumar, J.P. Singh, High-performance, temperature retardant and hydrophobic $BiCoO_3$:PDMS piezoelectric nanogenerator for effective energy harvesting in harsh environments, Chemical Engineering Journal, 532 (2026) 174311.

[6] J. Zou, Z. Jiang, J. Kim, C. Wu, J. Park, Performance enhancement of BaTiO3-PDMS flexible piezoelectric nanogenerator using double ZTO microsphere monolayers, Ceramics International, (2026).

[7] K. Shi, Y. Zhang, S. Taleb, H. Phillips-Brene, E. Wilhelm, M. Acuautla, Boosted output of flexible PANI@BTO/PVDF–TrFE piezoelectric nanogenerators for self-powered

View Article Online
DOI: 10.1039/D6LP00034G

multifunctional sensing in wearable systems, Chemical Engineering Journal, 535 (2026) 175420.

[8] K. Kukreja, S. Pratihar, P.K. Panda, P.K. S Mural, High-performance piezoelectric nanogenerator based on PVDF/2D layered Mo_3AlC_2 composites for sustainable energy harvesting applications, Sensors and Actuators A: Physical, 399 (2026) 117415.

[9] J.-H. Lee, K.Y. Lee, M.K. Gupta, T.Y. Kim, D.-Y. Lee, J. Oh, C. Ryu, W.J. Yoo, C.-Y. Kang, S.-J. Yoon, J.-B. Yoo, S.-W. Kim, Highly Stretchable Piezoelectric-Pyroelectric Hybrid Nanogenerator, Advanced Materials, 26 (2014) 765-769.

[10] L. Persano, C. Dagdeviren, Y. Su, Y. Zhang, S. Girardo, D. Pisignano, Y. Huang, J.A. Rogers, High performance piezoelectric devices based on aligned arrays of nanofibers of poly(vinylidenefluoride-co-trifluoroethylene), Nature Communications, 4 (2013) 1633.

[11] Z. Zhang, C. Yao, Y. Yu, Z. Hong, M. Zhi, X. Wang, Mesoporous Piezoelectric Polymer Composite Films with Tunable Mechanical Modulus for Harvesting Energy from Liquid Pressure Fluctuation, Advanced Functional Materials, 26 (2016) 6760-6765.

[12] C. Sun, J. Shi, D.J. Bayerl, X. Wang, PVDF microbelts for harvesting energy from respiration, Energy & Environmental Science, 4 (2011) 4508-4512.

[13] D. Zabek, J. Taylor, E.L. Boulbar, C.R. Bowen, Micropatterning of Flexible and Free Standing Polyvinylidene Difluoride (PVDF) Films for Enhanced Pyroelectric Energy Transformation, Advanced Energy Materials, 5 (2015) 1401891.

[14] S. Horiuchi, Y. Tokura, Organic ferroelectrics, Nature Materials, 7 (2008) 357-366.

[15] W. Zhang, Q. Feng, E. Hosono, D. Asakura, J. Miyawaki, Y. Harada, Tetragonal Distortion of a BaTiO3/Bi0.5Na0.5TiO3 Nanocomposite Responsible for Anomalous Piezoelectric and Ferroelectric Behaviors, ACS Omega, 5 (2020) 22800-22807.

[16] C.-T. Pan, S.-Y. Wang, C.-K. Yen, A. Kumar, S.-W. Kuo, J.-L. Zheng, Z.-H. Wen, R. Singh, S.P. Singh, M.T. Khan, R.K. Chaudhary, X. Dai, A. Chandra Kaushik, D.-Q. Wei, Y.-

L. Shiue, W.-H. Chang, Polyvinylidene Fluoride-Added Ceramic Powder Composite Near-Field Electrospinned Piezoelectric Fiber-Based Low-Frequency Dynamic Sensors, ACS Omega, 5 (2020) 17090-17101.

[17] S. Song, Y. Li, Q. Wang, C. Zhang, Boosting piezoelectric performance with a new selective laser sintering 3D printable PVDF/graphene nanocomposite, Composites Part A: Applied Science and Manufacturing, 147 (2021) 106452.

[18] Y. Xu, L. Jin, X. He, X. Huang, M. Xie, C. Wang, C. Zhang, W. Yang, F. Meng, J. Lu, Glowing stereocomplex biopolymers are generating power: polylactide/carbon quantum dot hybrid nanofibers with high piezoresponse and multicolor luminescence, Journal of Materials Chemistry A, 7 (2019) 1810-1823.

[19] Y. Mao, P. Zhao, G. McConohy, H. Yang, Y. Tong, X. Wang, Sponge-Like Piezoelectric Polymer Films for Scalable and Integratable Nanogenerators and Self-Powered Electronic Systems, Advanced Energy Materials, 4 (2014) 1301624.

[20] Y. Zhang, C.R. Bowen, S. Deville, Ice-templated poly(vinylidene fluoride) ferroelectrets, Soft Matter, 15 (2019) 825-832.

[21] T. Kowalchik, F. Khan, K. Le, P. Leland, S. Roundy, R. Warren, Effect of pore structure on the piezoelectric properties of barium titanate-polyvinylidene fluoride composite films, Nano Energy, 109 (2023) 108276.

[22] M. Hassanpour Amiri, K. Asadi, How Porosity Affects the Performance of Piezoelectric Energy Harvesters and Sensors, Advanced Physics Research, 2 (2023) 2200042.

[23] K. Okazaki, K. Nagata, Effects of Grain Size and Porosity on Electrical and Optical Properties of PLZT Ceramics, Journal of the American Ceramic Society, 56 (1973) 82-86.

[24] K. Ina, T. Mano, S.O. Nagata, Hydrophone Sensitivity of Porous Pb(Zr, Ti)O3 Ceramics, Japanese Journal of Applied Physics, 33 (1994) 5381.

[25] Y.-C. Chen, S. Wu, Piezoelectric composites with 3-3 connectivity by injecting polymer for hydrostatic sensors, Ceramics International, 30 (2004) 69-74.

[26] C.N. Della, D. Shu, The performance of 1–3 piezoelectric composites with a porous non-piezoelectric matrix, Acta Materialia, 56 (2008) 754-761.

[27] W.R. McCall, K. Kim, C. Heath, G. La Pierre, D.J. Sirbuly, Piezoelectric Nanoparticle–Polymer Composite Foams, ACS Applied Materials & Interfaces, 6 (2014) 19504-19509.

[28] B.A. Tuttle, J.E. Smay, J. Cesarano, J.A. Voigt, T.W. Scofield, W.R. Olson, J.A. Lewis, Robocast Pb(Zr0.95Ti0.05)O3 Ceramic Monoliths and Composites, Journal of the American Ceramic Society, 84 (2001) 872-874.

[29] M. Allahverdi, S.C. Danforth, M. Jafari, A. Safari, Processing of advanced electroceramic components by fused deposition technique, Journal of the European Ceramic Society, 21 (2001) 1485-1490.

[30] K. Boumchedda, M. Hamadi, G. Fantozzi, Properties of a hydrophone produced with porous PZT ceramic, Journal of the European Ceramic Society, 27 (2007) 4169-4171.

[31] H. Kara, R. Ramesh, R. Stevens, C.R. Bowen, Porous PZT ceramics for receiving transducers, IEEE Transactions on Ultrasonics, Ferroelectrics, and Frequency Control, 50 (2003) 289-296.

[32] V. Wilkens, W. Molkenstruck, Broadband PVDF Membrane Hydrophone for Comparisons of Hydrophone Calibration Methods up to 140 MHz, IEEE Transactions on Ultrasonics, Ferroelectrics, and Frequency Control, 54 (2007) 1784-1791.

[33] M. Toda, J. Dahl, PVDF corrugated transducer for ultrasonic ranging sensor, Sensors and Actuators A: Physical, 134 (2007) 427-435.

[34] S.J. Kang, Y.J. Park, I. Bae, K.J. Kim, H.-C. Kim, S. Bauer, E.L. Thomas, C. Park, Printable Ferroelectric PVDF/PMMA Blend Films with Ultralow Roughness for Low Voltage Non-Volatile Polymer Memory, Advanced Functional Materials, 19 (2009) 2812-2818.

[35] F. Wang, M. Tanaka, S. Chonan, Development of a PVDF Piezopolymer Sensor for Unconstrained In-Sleep Cardiorespiratory Monitoring, Journal of Intelligent Material Systems and Structures, 14 (2003) 185-190.

[36] L. Song, Z. Huang, S. Guo, Y. Li, Q. Wang, Hierarchically Architected Polyvinylidene Fluoride Piezoelectric Foam for Boosted Mechanical Energy Harvesting and Self-Powered Sensor, ACS Applied Materials & Interfaces, 13 (2021) 37252-37261.

[37] H.-Q. Liang, Q.-Y. Wu, L.-S. Wan, X.-J. Huang, Z.-K. Xu, Thermally induced phase separation followed by in situ sol–gel process: A novel method for PVDF/SiO2 hybrid membranes, Journal of Membrane Science, 465 (2014) 56-67.

[38] L. Song, R. Dai, Y. Li, Q. Wang, C. Zhang, Polyvinylidene Fluoride Energy Harvester with Boosting Piezoelectric Performance through 3D Printed Biomimetic Bone Structures, ACS Sustainable Chemistry & Engineering, 9 (2021) 7561-7568.

[39] J. Guo, Q. Wu, C. Zhang, Y. Li, M. Nie, Q. Wang, Y. Liu, Porosity manipulation to boost piezoelectric output via supercritical carbon dioxide foaming and surface modification, Materials & Design, 217 (2022) 110616.

[40] S. Badatya, D.K. Bharti, N. Sathish, A.K. Srivastava, M.K. Gupta, Humidity Sustainable Hydrophobic Poly(vinylidene fluoride)-Carbon Nanotubes Foam Based Piezoelectric Nanogenerator, ACS Applied Materials & Interfaces, 13 (2021) 27245-27254.

[41] Y. Zhao, S. Shi, Z. Ma, G. Li, X. Liao, Polymorphism regulation in poly(vinylidene fluoride) foam achieved by supercritical CO2 foaming assisted with ionic liquid for high-performance piezoelectric device, Composites Science and Technology, 261 (2025) 111031.

[42] J. Chen, L. Song, F. Qi, S. Qin, X. Yang, W. Xie, K. Gai, Y. Han, X. Zhang, Z. Zhu, H. Cai, X. Pei, Q. Wan, N. Chen, J. Wang, Q. Wang, Y. Li, Enhanced bone regeneration via ZIF-8 decorated hierarchical polyvinylidene fluoride piezoelectric foam nanogenerator: Coupling of bioelectricity, angiogenesis, and osteogenesis, Nano Energy, 106 (2023) 108076.

View Article Online
DOI: 10.1039/D6LP00034G

[43] Y. Zhao, B. Wang, S. Zeng, S. Shi, G. Li, X. Liao, β-phase formation of poly(vinylidene fluoride) foam based on the porous morphology control via supercritical carbon dioxide, Sustainable Materials and Technologies, 40 (2024) e00987.

[44] C. Ravikumar, V. Markevicius, Ferroelectret Polypropylene Foam-Based Piezoelectric Energy Harvester for Different Seismic Mass Conditions, Actuators, 2023, pp. 215.

[45] X. Chen, T. Ding, X. Wu, M. Qin, Q. Cai, H. Tai, Q. Li, Enhanced piezoelectric output performance in flexible polyvinylidene fluoride foam with a hierarchical dual-pore structure, Journal of Materials Chemistry C, 13 (2025) 13529-13541.

[46] X. Liu, X. Li, X. Wei, J. Chen, Y. Li, C. Zhang, Supercritical Fluid Foaming of Self-Polarized β-PVDF Piezoelectric Foam with Tailored Cells for Advanced Energy Harvesting, ACS Applied Materials & Interfaces, 17 (2025) 40499-40507.

View Article Online
DOI: 10.1039/D6LP00034G

The data supporting this article have been included as part of the Supplementary Information